Dispersion of seismic body waves in isotropic elastic mantle heterogeneity derived from a geodynamic model

Bernhard S. A. Schuberth[1], Christophe Zaroli[2] and Guust Nolet[3]

1) Dept. of Earth and Environmental Sciences, Ludwig-Maximilians-University Munich, Germany. 2) Institute de Physique du Globe de Strasbourg (Université de Strasbourg/EOST), France. 3) Géoazur, Université de Nice – Sophia Antipolis, France. Contact: mail@bernhard-schuberth.de

1. Abstract

Recently, we developed a new joint forward modeling approach to test geodynamic hypotheses directly against seismic data: Seismic heterogeneity is predicted by converting the temperature field of a high-resolution 3-D mantle circulation model (MCM) into seismic velocities using thermodynamic models of mantle mineralogy. 3-D global wave propagation in the synthetic elastic structures is then simulated using a spectral element method. Being based on forward modelling only, this approach allows us to generate synthetic wavefields and seismograms independently of seismic observations. This way, the danger of circular reasoning is minimized, which may pose problems when using tomographic mantle models in seismic forward calculations. In addition, our approach avoids the problems of limited resolution and non-uniqueness inherent in tomographic inversions while taking all possible finite-frequency effects into account.

In an earlier study, we focused on direct body waves and measured traveltime variations of the synthetic P- and S-waves at one single dominant period (15 seconds) using an automated cross-correlation technique. However, capturing the correct physics of wave propagation in mantle models that exhibit a realistic power spectrum of seismic heterogeneity provides us with a unique tool to study the effects of focusing/defocusing and diffraction. In particular, using our approach we are now able to analyse seismic dispersion in isotropic, purely elastic structures in a consistent manner. This can provide important information on the relative contributions of inherent (i.e., related to dissipation of seismic energy) and structural dispersion and may, for example, help in improving our understanding of seismic attenuation. To this end, we extended our earlier work and measured P- and S-wave delay times now in four different frequency bands. This way, we created a synthetic finite-frequency traveltime dataset that can be compared to the existing global datasets derived from seismic observations.

2. Key Questions

What are the dispersion characteristics of purely elastic isotropic mantle heterogeneity?

The realistic length-scales of structure in our model allow for an analysis beyond studying random media

How do they compare to those of observations and tomographic models?

Can seismic dispersion be used to test geodynamic hypotheses?

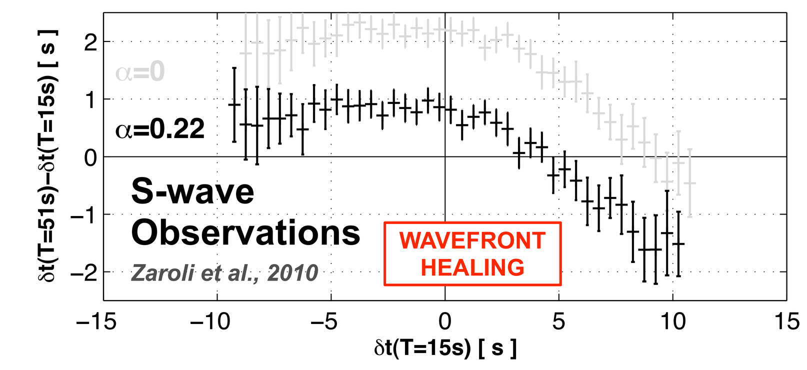

Fig. 1. Plot of the mean difference between observed S-wave traveltime variations measured at long periods (51 s dominant period) and short periods (15 s dominant period) as a function of the delay times at short periods. A clear trend is visible for slow arrivals, which show increasing differences with increasing short period delay times. This indicates wavefront healing in the data; that is, the long-period traveltime variations are (on average) smaller in magnitude than the short-period traveltime variations [Zaroli et al, 2010].

3. Approach - Joint Forward Modelling

Mantle Dynamics → Mineralogy → 3-D Elastic Structure → Wave Propagation → Synthetic Seismic Data

3-D Mantle Circulation Modelling
Constrains temperature field
T is not a free parameter

Thermodynamic Models + Composition
Link temperature to elastic parameters

Model Planet
Seismic heterogeneity

Spectral Element Method

Full Waveforms
Independent of seismic observations!

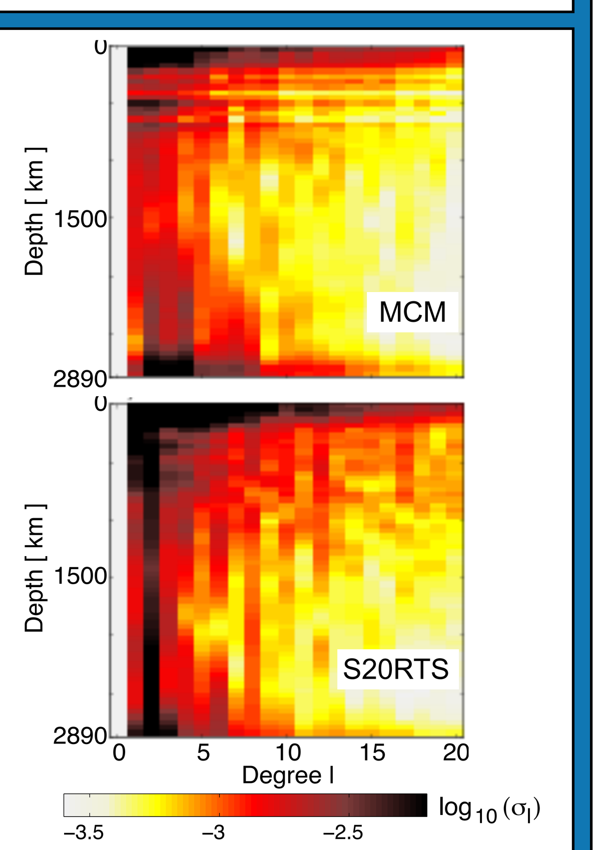

Fig. 2. Comparison of characteristic length-scales in the MCM (tomographically filtered) and S20RTS [Ritsema et al., 2004]. Plotted is the spectral power of heterogeneity on a logarithmic scale as a function of spherical harmonic degree and depth [Schuberth et al., 2009a].

4. Wave Propagation in a Synthetic Earth

Wavefield with 10 s shortest period
SPECFEM3D Globe
Komatitsch & Tromp 2002a

Traveltime delays
Full waveform cross-correlation
Four frequency bands
15, 22, 34 and 51 s dominant period
Finite-frequency interpretation

Isotropic 3-D mantle heterogeneity only
1-D crust, no attenuation, no anisotropy, etc.

Homogeneous data coverage
34 earthquakes
42250 equidistant virtual station

~6,000,000 P- and S-wave measurements

Fig. 3. Snapshots of the three-dimensional wavefield in our geodynamic model. 3-D global wave propagation was simulated for an earthquake in the Fiji Islands region using a spectral element technique. The wavefield is depicted by green and magenta colours together with the shear wave velocity variations in the model, for which vertical cross-sections and iso-surfaces are shown on a blue to brownish colour scale ranging from -2 to 2 per cent. Surface topography is also shown for parts of the globe for geographic reference [Schuberth et al. 2012].

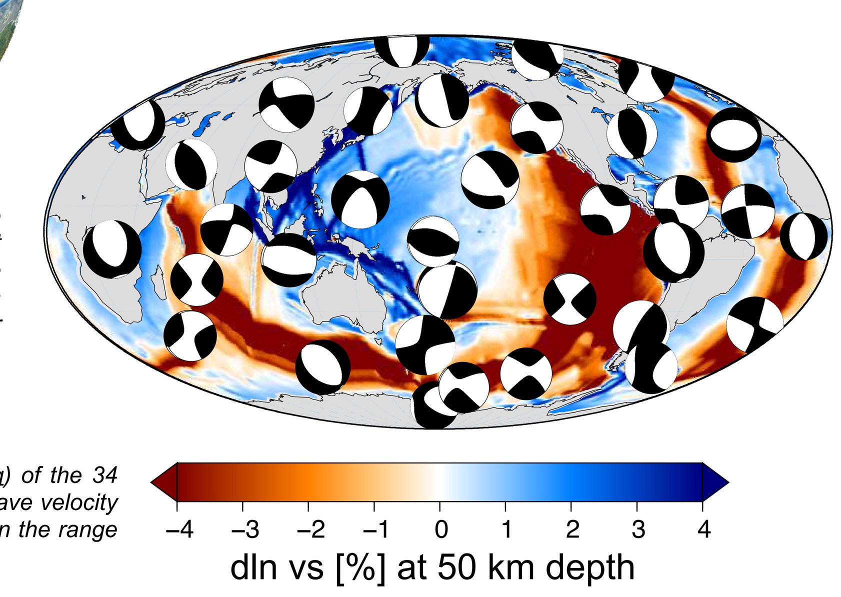

Fig. 4. Locations and Harvard moment tensor solutions (www.globalcmt.org) of the 34 earthquakes used in this study. The events are plotted on top of the shear wave velocity perturbations from our model at a depth of 50 km. Moment magnitudes are in the range from 5.3 to 7.0.

5. Synthetic Multi-Frequency Traveltime Variations

Traveltime delays are dominated by the near surface structure

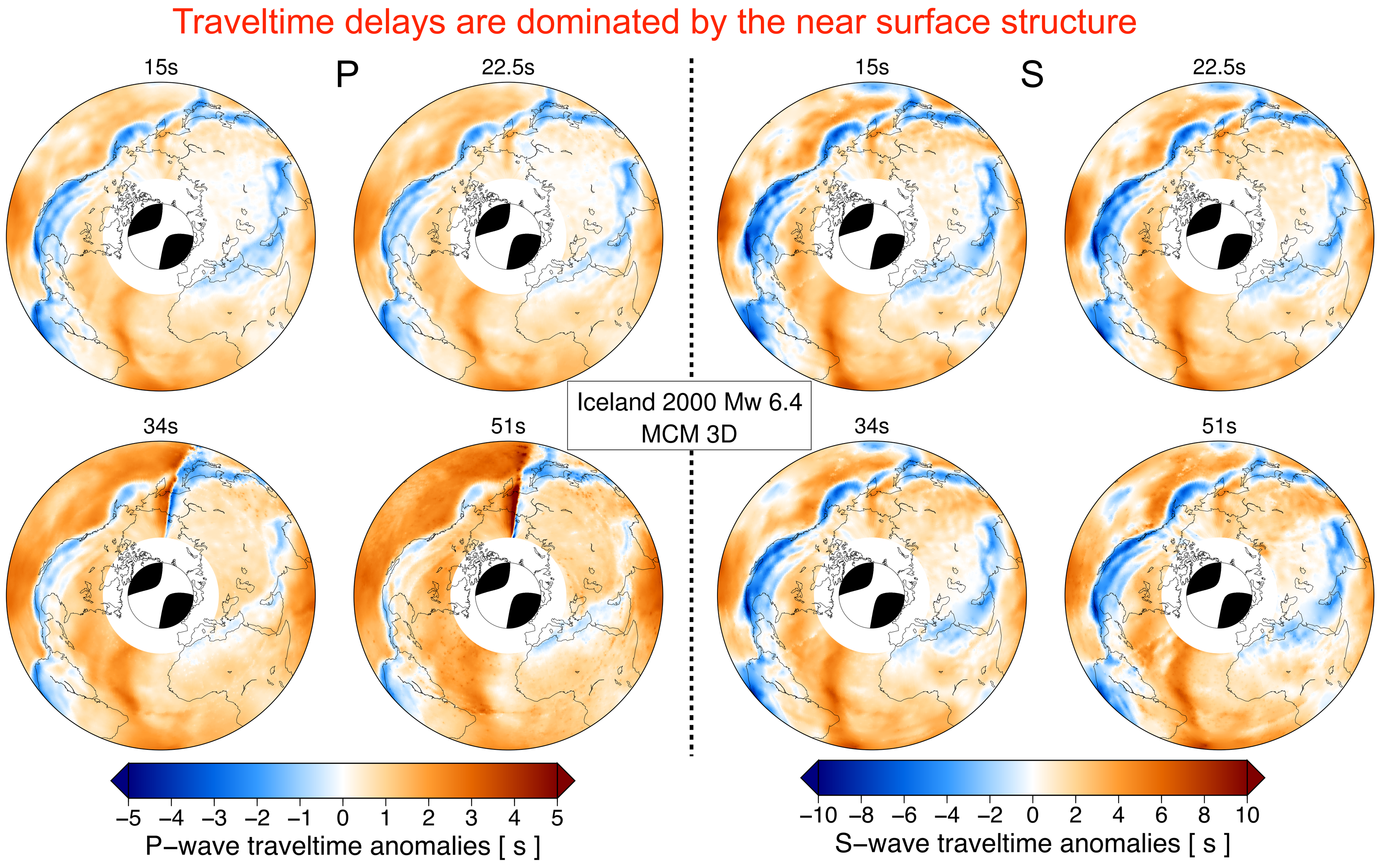

Fig. 5. Maps of traveltime variations, measured by cross-correlation of full waveform synthetic seismograms. Left: Traveltime variations of direct P-waves measured in four different frequency bands (15, 22.5, 34 and 51 s dominant period). Right: Same for S-waves. Traveltime anomalies are plotted at their respective receiver locations. A minimum epicentral distance range of 30° is used to guarantee a clear separation of the direct phases from later arrivals and to avoid problems due to upper-mantle triplications. Note the different colour scales for P- and S-waves and the dominance of positive delay times (a consequence of the event being located in a slow region).

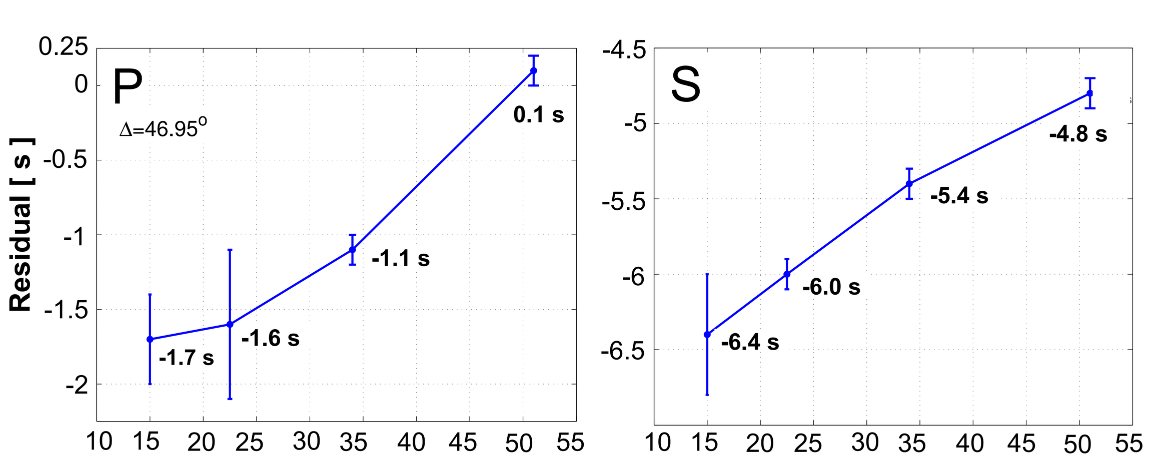

Fig. 6. Example of finite-frequency traveltime delays measured by cross-correlation of time windows selected by the automated software of Zaroli et al. [2010]. Measurements were performed at four different frequencies (15, 22, 34 and 51 seconds dominant period) using overlapping Gaussian filters. Left: P-wave measurements obtained from the vertical component ``record'' of a shallow event at the central mid-Atlantic ridge. Right: SH-wave measurements obtained from the transverse component. The decreasing magnitude of the negative delay times with increasing period results from dispersion of the seismic waves solely due to 3-D heterogeneity, as the effect of anelasticity was not included in the simulation.

6. Dispersion Characteristics of MCMs

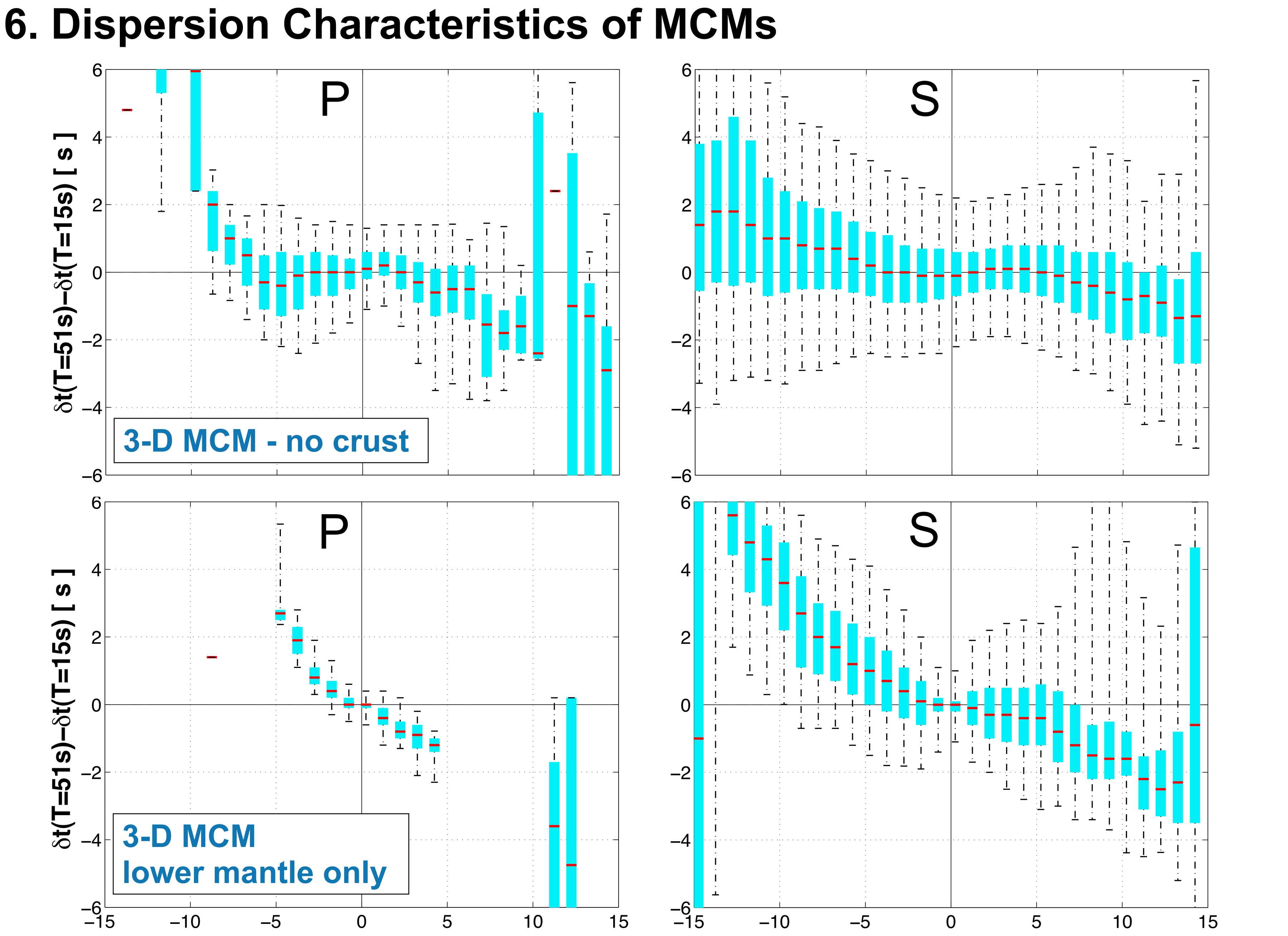

Fig. 7. Plots of the mean difference between synthetic traveltime variations measured at long periods (51 s dominant period) and short periods (15 s dominant period) as a function of the delay times at short periods (red line: median; cyan box: 25 and 75 percentiles; whiskers: 5 and 95 percentiles). Left panels: P-wave traveltime variations. Right panels: S-wave traveltime variations. Top row: Original MCM (i.e., 3-D heterogeneity in the entire mantle). Bottom row: Modified model where 3-D heterogeneity is present only below 800 km depth. Dispersion is visible in both models, but stronger in the modified model. Differences between long and short periods increase with increasing short period delay times (for both positive and negative delays). This indicates wavefront healing in the synthetic data; that is, the long-period traveltime variations are (on average) smaller in magnitude than the short-period traveltime delays. Note that the seismic velocities in both models are isotropic and purely elastic (i.e.; attenuation of seismic energy due to intrinsic dissipation was deliberately excluded in the wave propagation simulations).

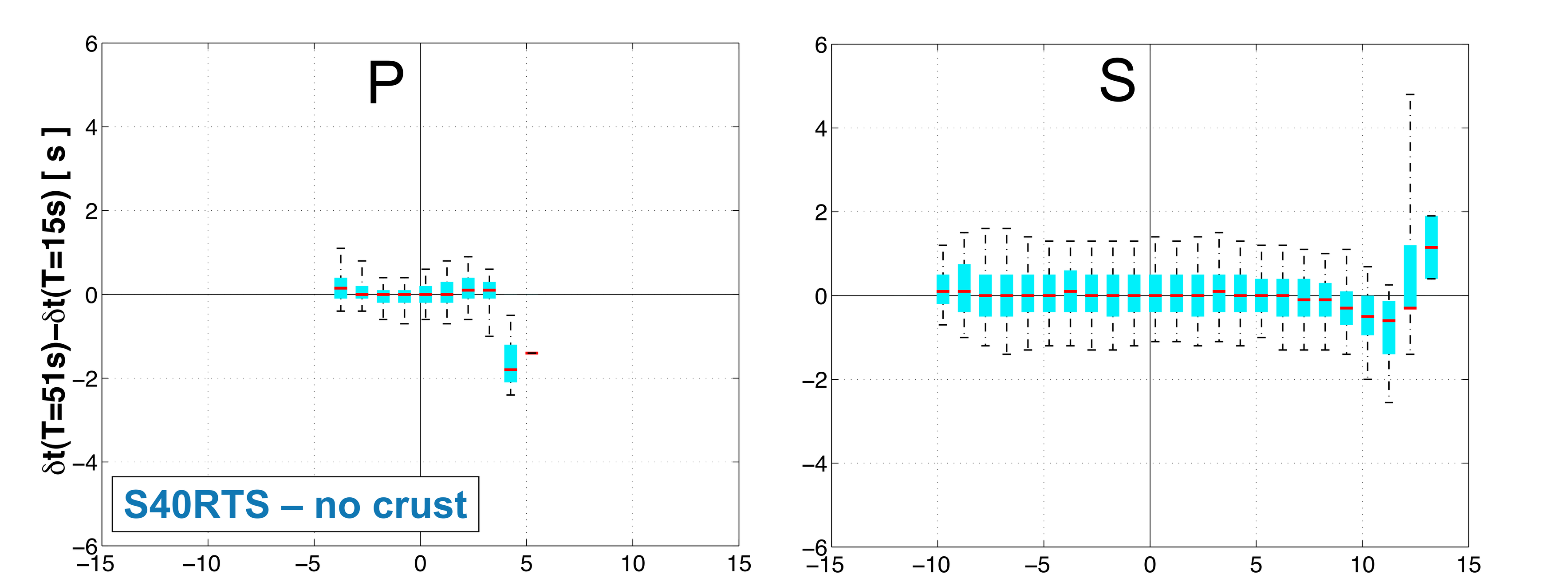

Fig. 8. Same as Figure 7 for tomographic model S40RTS [Ritsema et al., 2011]. Here, wavefront healing effects are smaller than in our MCM and the observations.

7. Conclusions and Outlook

Fully synthetic wavefields from joint modelling
Mantle flow + mineral physics + 3-D seismic wave propagation

Clear dispersion signal in our mantle circulation model
But not as strong as seen in the observations

Larger effect if heterogeneity is present only in the lower mantle
What are the effects of the lithosphere?
(Currently over-simplified representation in the MCM as pure thermal boundary layer)

Short-scale versus large-scale heterogeneity?
What are the dispersion characteristics of large chemical piles in the lower mantle?

Acknowledgements

BSAS was supported by a Marie Curie Intra European Fellowship within the 7th European Community Framework Programme [FP7/2007-2013] under grant agreement no. 235861. GN and CZ received support from the European Research Council (ERC Advanced grant 226837). The authors thank the Leibniz Supercomputing Centre for access to computing resources on HLRBII and the DEISA Consortium (www.deisa.eu), co-funded through the EU FP6 project RI-031513 and the FP7 project RI-222919, for support within the DEISA Extreme Computing Initiative.

References

1. Komatitsch, D. & Tromp, J., Geophys. J. Int., 149, 390–412, **2002a**.
2. Ritsema, J., van Heijst, H.J. & Woodhouse, J.H., J. geophys. Res., 109(B2), B02302, **2004**.
3. Ritsema J., van Heijst H.J., Deuss A., Woodhouse J.H., Geophys. J. Int., 184, **2011**.
4. Schuberth, B.S.A., Bunge, H.-P. & Ritsema, J., Geochem. Geophys. Geosyst., 10(5), Q05W03, **2009a**.
5. Schuberth, B.S.A., Zaroli, C. and G. Nolet, Geophys. J. Int., 188(3), 1393-1412, **2012**.
6. Zaroli C., Debayle E. & Sambridge M., Geophys. J. Int., 182, 1025-1042, **2010**.